

Biaxially textured cobalt-doped BaFe₂As₂ films with high critical current density over 1 MA/cm² on MgO-buffered metal-tape flexible substrates

Takayoshi Katase¹, Hidenori Hiramatsu¹, Vladimir Matias², Chris Sheehan², Yoshihiro Ishimaru³, Toshio Kamiya¹, Keiichi Tanabe³, and Hideo Hosono^{1,4,*}

¹ Materials and Structures Laboratory, Tokyo Institute of Technology, 4259 Nagatsuta-cho, Midori-ku, Yokohama 226-8503, Japan

² Superconductivity Technology Center, Los Alamos National Laboratory, Los Alamos, NM 87545, USA

³ Superconductivity Research Laboratory, International Superconductivity Technology Center, 10-13 Shinonome 1-chome, Koto-ku, Tokyo 135-0062, Japan

⁴ Frontier Research Center, Tokyo Institute of Technology, S2-6F East, 4259 Nagatsuta-cho, Midori-ku, Yokohama 226-8503, Japan

PACS No: 74.70.Dd, 74.25.Sv, 74.25.Qt, 84.71.Mn, 74.25.Fy, 81.15.Fg, 81.15.Kk

ABSTRACT

High critical current densities (J_c) > 1 MA/cm² were realized in cobalt-doped BaFe₂As₂ (BaFe₂As₂:Co) films on flexible metal substrates with biaxially-textured MgO base-layers fabricated by an ion-beam assisted deposition technique. The BaFe₂As₂:Co films showed small in-plane crystalline misorientations ($\Delta\phi_{\text{BaFe}_2\text{As}_2:\text{Co}}$) of $\sim 3^\circ$ regardless of twice larger misorientations of the MgO base-layers ($\Delta\phi_{\text{MgO}} = 7.3^\circ$), and exhibited high self-field J_c up to 3.5 MA/cm² at 2 K. These values are comparable to that on MgO single crystals and the highest J_c among iron pnictide superconducting tapes and wires ever reported. High in-field J_c suggests the existence of c -axis correlated vortex pinning centers.

Footnotes:

(*) Electronic mail: hosono@msl.titech.ac.jp

Iron-pnictide superconductors¹ possess potential for next-generation superconducting tapes or wires because of their relatively high critical temperatures (T_c) up to 56 K^{2,3} and high upper critical magnetic fields (H_{c2}/c) > 100 T with small anisotropy $\gamma (= H_{c2}/ab / H_{c2}/c) = 1-5$ ⁴⁻⁷. The most important factor for the practical application using high T_c materials including cuprates such as YBaCu₃O_{7- δ} (YBCO) has been the critical current density (J_c) through misaligned grain boundaries (GBs)⁸. The GB properties of the iron pnictides have been examined in cobalt-doped BaFe₂As₂ (BaFe₂As₂:Co) epitaxial films grown on bicrystal substrates with respect to misorientation angles (θ_{GB}) under high magnetic fields⁹ and a self-field¹⁰, because high $J_c > 1$ MA/cm² have been achieved only in BaFe₂As₂:Co¹¹⁻¹³ among thin films of the iron pnictides; these studies have led to recent demonstrations of thin film superconducting devices such as Josephson junctions^{14,15} and a SQUID¹⁶. The BaFe₂As₂:Co bicrystal GBs exhibit high self-field J_c unchanged at > 1 MA/cm² at 4 K up to a large critical GB angle (θ_c) of 9°¹⁰, which is approximately twice larger than that of YBCO. We confirmed that this difference from YBCO originates from the intrinsic natures of the iron pnictides such as the metallic nature of GB regions that would be carrier-depleted iron pnictides¹⁰.

To date, iron pnictide superconducting wires have been examined mainly by a powder-in-tube technique¹⁷, but their highest J_c are still as low as $\sim 1.0 \times 10^4$ A/cm² at 4.2 K and the decay slopes with H are large¹⁸. These deteriorated properties suffer from segregation of secondary phases at GBs, reaction with sheath materials, and/or difficulty in biaxial alignment of the crystallite orientations. Therefore, it is desirable to use ion-beam assisted deposition (IBAD) substrates to prepare biaxially textured films with in-plane misorientation angles $\leq 9^\circ$ on flexible polycrystalline metal substrates, which

have led to high J_c for YBCO coated conductors¹⁹. The IBAD technique is now widely used to grow biaxially-textured MgO buffer layers with in-plane misorientation angles $\Delta\phi_{\text{MgO}} = 6\text{--}8^\circ$ ^{20,21}. For YBCO coated conductors, additional buffer layers such as LaMnO_3 and CeO_2 are often used to achieve $\Delta\phi \leq 5^\circ$ to grow high-quality YBCO films^{22,23} because YBCO exhibits steep deterioration in J_c with increasing $\Delta\phi_{\text{YBCO}} \geq 5^\circ$ ²⁴, although YBCO coated conductors with $\Delta\phi_{\text{YBCO}} = \sim 2^\circ$ can be grown directly on simpler IBAD-MgO templates if very thick ($>1 \mu\text{m}$) YBCO films are grown along with a reactive co-evaporation technique²⁵.

Recently, Iida et al.²⁶ reported higher J_c ($\sim 0.1 \text{ MA/cm}^2$ at 8 K) in the epitaxially-grown $\text{BaFe}_2\text{As}_2\text{:Co}$ films on IBAD-MgO buffered metal substrates with an additional Fe buffer layer; however, the J_c values are still substantially lower than those on MgO single-crystal substrates ($\sim 0.5 \text{ MA/cm}^2$). Moreover, the ferromagnetic Fe layer would not be appropriate for applications to alternating current devices.

In this letter, we report a high self-field J_c over 1 MA/cm^2 at $T \leq 10 \text{ K}$, which is an order of magnitude higher than those reported to date for iron pnictide tapes²⁶ and comparable to those of epitaxial films on various single crystals^{11–13}, in $\text{BaFe}_2\text{As}_2\text{:Co}$ films fabricated on IBAD-MgO buffered metal-tape substrates (IBAD substrates). An interesting growth mode was observed; i.e., the $\text{BaFe}_2\text{As}_2\text{:Co}$ films were grown directly on MgO base-layers with large $\Delta\phi_{\text{MgO}}$ of $5.5\text{--}7.3^\circ$, but their $\Delta\phi_{\text{BaFe}_2\text{As}_2\text{:Co}}$ became much smaller $\sim 3^\circ$ even for the small film thickness' of $\leq 220 \text{ nm}$, which is largely different from the YBCO cases and would be essential for the high J_c .

$\text{BaFe}_2\text{As}_2\text{:Co}$ films were fabricated on IBAD substrates by pulsed laser deposition¹². The IBAD substrates consisted of top electron-beam-deposited homo-epitaxial MgO layer/IBAD textured MgO layer/amorphous Y_2O_3 planarizing bed

layer/bottom Hastelloy C-276 polycrystalline metal tape. Detailed processes for the IBAD substrates including the planarization process are described in ref. 27. Here, we employed three different IBAD substrates with $\Delta\phi_{\text{MgO}} = 7.3^\circ$, 6.1° and 5.5° ($\Delta\phi_{\text{MgO}}$ is evaluated as the in-plane full-width at half maximum (FWHM) value of a MgO 022 rocking curve). We used thin MgO base-layers (homo-epitaxial MgO/IBAD-MgO layers) less than 170 nm, though $\Delta\phi_{\text{MgO}} < 4^\circ$ can be obtained if thicker homo-epitaxial MgO layers are grown²¹. All the substrates were cut from a long tape to $1 \times 1 \text{ cm}^2$ pieces. The root-mean-square values of the surface roughness of all the homo-epitaxially grown MgO top layers were $\sim 1.5 \text{ nm}$. Each film thickness (130–220 nm) was confirmed by cross-sectional field-emission scanning electron microscopy (FE-SEM). As shown in Fig. 1(a), the thickness of the BaFe₂As₂:Co layer and the MgO base-layer with $\Delta\phi_{\text{MgO}} = 6.1^\circ$ are confirmed to be 150 nm and 50 nm, respectively. Film structures including crystalline quality and crystallites orientation were examined by x-ray diffraction (XRD, anode radiation: CuK α_1) at room temperature. Temperature (T) dependences of electrical resistivity, $\rho(T)$, and the transport J_c were measured by a four-probe dc method for 300 μm -long, 10 μm -wide micro-bridge patterns formed by photolithography and Ar-ion milling. The J_c was defined from current density–voltage (J – V) characteristics with a criterion of 1 $\mu\text{V}/\text{cm}$ electric field. H dependence of J_c ($J_c(H)$) was evaluated up to $\mu_0 H = 9 \text{ T}$ applied parallel or perpendicular to the film surface.

Figures 1(b) shows the out-of-plane XRD patterns for (i) a BaFe₂As₂:Co epitaxial film on a MgO single crystalline substrate (Film/sc-MgO), (ii) a BaFe₂As₂:Co film on a IBAD substrate (Film/IBAD) with $\Delta\phi_{\text{MgO}} = 5.5^\circ$, and (iii) a bare IBAD substrate. The out-of-plane XRD pattern of Film/IBAD exhibits intense 00 l and weak

110 diffractions assigned to the BaFe₂As₂:Co phase. Besides the MgO 002 diffraction peak, a weak diffraction of Fe impurity is also observed, which is similar to the XRD patterns of Film/sc-MgO. The other small peaks originate from the IBAD substrates, and a diffraction of Y₂O₃ appears at ~29° because the Y₂O₃ layer slightly crystallized during the high temperature growth of the BaFe₂As₂:Co films. Inset figure in Fig. 1(b)(ii) shows an out-of-plane rocking curve corresponding to the BaFe₂As₂:Co 004 diffraction for Film/IBAD. The FWHM of the rocking curve was $\Delta\omega = 1.5^\circ$, indicating highly *c*-axis orientated films.

In order to evaluate the in-plane orientation relationship between the BaFe₂As₂:Co top-layer and the MgO base-layer, pole-figure measurements were performed for the 103 diffractions of BaFe₂As₂:Co and the 022 of MgO. Figure 1(c) shows β scan results for the BaFe₂As₂:Co layer and the MgO base-layer with $\Delta\phi_{\text{MgO}} = 5.5^\circ$. Both the patterns exhibit the fourfold rotational symmetry with the same peak angles, which confirms biaxially textured growth of the BaFe₂As₂:Co films on the MgO base-layers with the relationship of (001)[100] BaFe₂As₂:Co// (001)[100] MgO.

Figure 1(d) shows the $\Delta\phi$ relation between the BaFe₂As₂:Co top-layers and the MgO base-layers. The BaFe₂As₂:Co layers show small misorientation angles of $\Delta\phi_{\text{BaFe}_2\text{As}_2:\text{Co}} = 3.2\text{--}3.5^\circ$ regardless of the larger $\Delta\phi_{\text{MgO}}$ (5.5–7.3°) of the MgO base-layers. Such a significant improvement in the in-plane orientation of the BaFe₂As₂:Co top-layer compared with the MgO base-layer may be explained by a “self-epitaxy” effect. It would be noteworthy that the reduction rate in $\Delta\phi_{\text{BaFe}_2\text{As}_2:\text{Co}}$ with respect to the film thickness is much faster for BaFe₂As₂:Co than that observed in YBCO films²⁸.

Figure 2 shows $\rho(T)$ curves for Film/IBAD and Film/sc-MgO. The onset T_c and the superconducting transition width ΔT_c for Film/IBAD were 22.0 K and 1.5 K,

respectively, and those for Film/sc-MgO were 21.0 K and 1.5 K. The broader transition starting from 26.4 K for Film/IBAD is probably due to inhomogeneous Co content in the film, which would be caused by inhomogeneity in the substrate temperature due to the flexibility of the IBAD substrates. J - V characteristics at 2 K for Film/IBAD with $\Delta\phi_{\text{MgO}} = 7.3^\circ$, 6.1° and 5.5° are shown in the inset of Fig. 2. All the J - V curves showed sharp superconducting transitions without weak-link behavior at the GBs. Self-field J_c values of 3.6, 1.6 and 1.2 MA/cm² were obtained for Film/IBAD with $\Delta\phi_{\text{MgO}} = 7.3^\circ$, 6.1° and 5.5° , respectively. This result also shows that the difference in $\Delta\phi_{\text{MgO}}$ of MgO base-layers did not affect these self-field J_c because the in-plane orientations of the BaFe₂As₂:Co films are similar ($\Delta\phi_{\text{BaFe}_2\text{As}_2:\text{Co}} = \sim 3^\circ$). The J_c values of the BaFe₂As₂:Co films on the IBAD substrates are comparable to that on MgO single crystals and remains at ≥ 1 MA/cm² at $T \leq 10$ K, which is consistent with the fact that the $\Delta\phi_{\text{BaFe}_2\text{As}_2:\text{Co}}$ are much smaller than the critical GB misorientation angle ($\theta_c = 9^\circ$) reported in ref. 10.

Figure 3 shows the $J_c(H//c)$ characteristics at $T = 4$ K and 12 K for Film/IBAD with $\Delta\phi_{\text{MgO}} = 6.1^\circ$. Those of the Film/sc-MgO¹⁰ are also shown for comparison. All the $J_c(H//c)$ curves monotonically decrease with increasing H , but the slopes (dJ_c/dH) for Film/IBAD are smaller than those for Film/sc-MgO, which would originate from a stronger vortex pinning effect along the c -axis and also from the higher T_c with high irreversibility field of the Film/IBAD. Figure 3 (b) shows the $J_c(H//ab)$ and $J_c(H//c)$ dependences at 4–18 K for Film/IBAD with $\Delta\phi_{\text{MgO}} = 6.1^\circ$. $J_c(H//ab)$ is larger than $J_c(H//c)$ in almost the whole H range at 4 K, while crossovers are observed at 5.0 T at 12 K and 2.9 T at 16 K, respectively. At a higher T of 18 K, $J_c(H//c)$ is greater than $J_c(H//ab)$ in the whole H region. These results are different from the $J_c(H)$ curves for

BaFe₂As₂:Co single crystals, which show the relation of $J_c(H//ab) > J_c(H//c)$ in the whole H and T region²⁹ that is reasonable based on the intrinsic anisotropy of H_{c2} (i.e.; $H_{c2//ab} > H_{c2//c}$)⁶. These results suggest the existence of strong vortex pinning centers along the c -axis in Film/IBAD, which is effective at high $T \geq 12$ K in the low H region less than several T. The inset figure plots the pinning force density $F_p = J_c \times \mu_0 H$ as a function of H measured in $H//c$ at $T = 4$ – 18 K. Each F_p curve takes a peak (F_{pmax}) as indicated by arrows in the inset at $T \geq 12$ K. The largest F_{pmax} is ~ 8 GN/m³ at 4 K but is three times smaller than those of BaFe₂As₂:Co epitaxial films on LSAT single crystals (30 GN/m³ at ~ 12 T)³⁰. It suggests that much higher in-field J_c would be realized on IBAD substrates by further optimizing the c -axis correlated pinning centers.

In conclusion, we demonstrated high self-field $J_c = 1.2$ – 3.6 MA/cm² at 2 K for BaFe₂As₂:Co films directly grown on IBAD-MgO buffered flexible metal substrates. The biaxially-textured BaFe₂As₂:Co films exhibited excellent in-plane alignment with $\Delta\phi_{\text{BaFe}_2\text{As}_2:\text{Co}} \sim 3^\circ$ regardless of the larger $\Delta\phi_{\text{MgO}} = 5.5$ – 7.3° of the MgO base-layers. The in-field J_c of the BaFe₂As₂:Co films on the IBAD substrates is substantially higher than that for BaFe₂As₂:Co films on MgO single crystals, probably due to c -axis vortex pinning effects. These results imply that high J_c coated conductors can be fabricated with BaFe₂As₂:Co using less-well-textured templates and with large $\Delta\phi$, which allows for a simple and low-cost process for high- J_c , high- H_c superconducting tapes.

Acknowledgment

This work was supported by the Japan Society for the Promotion of Science (JSPS), Japan, through the “Funding Program for World-Leading Innovative R&D on Science and Technology (FIRST) Program”.

REFERENCES

1. Y. Kamihara, T. Watanabe, M. Hirano, and H. Hosono, *J. Am. Chem. Soc.* **130**, 3296 (2008).
2. X. -H. Chen, T. Wu, G. Wu, R. H. Liu, H. Chen, and D. F. Fang, *Nature* **453**, 761 (2008).
3. C. Wang, L. Li, S. Chi, Z. Zhu, Z. Ren, Y. Li, Y. Wang, X. Lin, Y. Luo, S. Jiang, X. Xu, G. Cao, and Z. Xu, *EPL* **83**, 67006 (2008).
4. F. Hunte, J. Jaroszynski, A. Gurevich, D. C. Larbalestier, R. Jin, A. S. Sefat, M. A. McGuire, B. C. Sales, D. K. Christen, and D. Mandrus, *Nature* **453**, 903 (2008).
5. H. Q. Yuan, J. Singleton, F. F. Balakirev, S. A. Baily, G. F. Chen, J. L. Luo, and N. L. Wang, *Nature* **457**, 565 (2009).
6. A. Yamamoto, J. Jaroszynski, C. Tarantini, L. Balicas, J. Jiang, A. Gurevich, D. C. Larbalestier, R. Jin, A. S. Sefat, M. A. McGuire, B. C. Sales, D. K. Christen, and D. Mandrus, *Appl. Phys. Lett.* **94**, 062511 (2009).
7. S. A. Baily, Y. Kohama, H. Hiramatsu, B. Maiorov, F. F. Balakirev, M. Hirano, and H. Hosono, *Phys. Rev. Lett.* **102**, 117004 (2009).
8. D. Larbalestier, A. Gurevich, D. M. Feldmann, and A. Polyanskii, *Nature* **414**, 368 (2001).
9. S. Lee, J. Jiang, J. D. Weiss, C. M. Folkman, C. W. Bark, C. Tarantini, A. Xu, D. Abraimov, A. Polyanskii, C. T. Nelson, Y. Zhang, S. H. Baek, H. W. Jang, A. Yamamoto, F. Kametani, X. Q. Pan, E. E. Hellstrom, A. Gurevich, C. B. Eom, and D. C. Larbalestier, *Appl. Phys. Lett.* **95**, 212505 (2009).
10. T. Katase, Y. Ishimaru, A. Tsukamoto, H. Hiramatsu, T. Kamiya, K. Tanabe and H. Hosono, arXiv: 1011.5721 (unpublished).
11. S. Lee, J. Jiang, C. T. Nelson, C. W. Bark, J. D. Weiss, C. Tarantini, H. W. Jang, C. M. Folkman, S. H. Baek, A. Polyanskii, D. Abraimov, A. Yamamoto, Y. Zhang, X. Q. Pan, E. E. Hellstrom, D. C. Larbalestier, and C. B. Eom, *Nat. Mater.* **9**, 397 (2010).
12. T. Katase, H. Hiramatsu, T. Kamiya, and H. Hosono, *Appl. Phys. Express* **3**, 063101 (2010).

13. D. Rall, K. Il'in, K. Iida, S. Haindl, F. Kurth, T. Thersleff, L. Schultz, B. Holzapfel, and M. Siegel, *Phys. Rev. B* **83**, 134514 (2011).
14. T. Katase, Y. Ishimaru, A. Tsukamoto, H. Hiramatsu, T. Kamiya, K. Tanabe and H. Hosono, *Appl. Phys. Lett.* **96**, 142507 (2010).
15. S. Schmidt, S. Döring, F. Schmidl, V. Grosse, P. Seidel, K. Iida, F. Kurth, S. Haindl, I. Mönch, and B. Holzapfel, *Appl. Phys. Lett.* **97**, 172504 (2010).
16. T. Katase, Y. Ishimaru, A. Tsukamoto, H. Hiramatsu, T. Kamiya, K. Tanabe and H. Hosono, *Supercond. Sci. Technol.* **23**, 082001 (2010).
17. Z. Gao, L. Wang, Y. Qi, D. Wang, X. Zhang, and Y. Ma, *Supercond. Sci. Technol.* **21**, 105024 (2008).
18. K. Togano, A. Matsumoto, and H. Kumakura, *Appl. Phys. Express* **4**, 043101 (2011).
19. Y. Iijima, N. Tanabe, O. Kohno, and Y. Ikeno, *Appl. Phys. Lett.* **60**, 769 (1992).
20. C. P. Wang, K. B. Do, M. R. Beasley, T. H. Geballe, and R. H. Hammond, *Appl. Phys. Lett.* **71**, 2955 (1997).
21. V. Matias, J. Hänisch, E. J. Rowley, and K. Güth, *J. Mater. Res.* **24**, 125 (2009).
22. Y. Yamada, S. Miyata, M. Yoshizumi, H. Fukushima, A. Ibi, A. Kionoshita, T. Izumi, Y. Shiohara, T. Kato, and T. Hirayama, *IEEE Trans Appl. Supercond.* **19**, 3236 (2009).
23. M. P. Paranthaman, T. Aytug, S. Kang, R. Feenstra, J. D. Budai, D. K. Christe, P. N. Arendt, L. Stan, J. R. Groves, R. F. DePaula, S. R. Foltyn, and T. G. Holesinger, *IEEE Trans Appl. Supercond.* **13**, 2481 (2003).
24. H. Hilgenkamp, and J. Mannhart, *Rev. Mod. Phys.* **74**, 485 (2002).
25. V. Matias, E. J. Rowley, Y. Coulter, B. Maiorov, T. Holesinger, C. Yung, V. Glyantsev, and B. Moeckly, *Supercond. Sci. Technol.* **23**, 014018 (2010).
26. K. Iida, J. Hänisch, S. Trommler, V. Matias, S. Haindl, F. Kurth, I. Lucas del Pozo, R. Hühne, M. Kidszun, J. Engelmann, L. Schultz, and B. Holzapfel, *Appl. Phys. Express* **4**, 013103 (2011).
27. C. Sheehan, Y. Jung, T. Holesinger, D. M. Feldmann, C. Edney, J. F. Ihlefeld, P. G. Clem, and V. Matias, *Appl. Phys. Lett.* **98**, 071907 (2011).
28. V. Matias, B. J. Gibbons, J. Hänisch, R. J. A. Steenwelle, P. Dowden, J. Rowley, J. Y. Coulter, and D. Peterson, *IEEE Trans. Appl. Supercond.* **17**, 3263 (2007).

29. M. A. Tanatar, N. Ni, C. Martin, R. T. Gordon, H. Kim, V. G. Kogan, G. D. Samolyuk, S. D. Bud'ko, P. C. Canfield, and R. Prozorov, *Phys. Rev. B* **79**, 094507 (2009).
30. B. Maiorov, T. Katase, S. A. Baily, H. Hiramatsu, T. G. Holesinger, H. Hosono, and L. Civale, *Supercond. Sci. Technol.* **24**, 055007 (2011).

Figure captions

FIG. 1. (Color online) (a) Cross-sectional FE-SEM image of BaFe₂As₂:Co film directly grown on IBAD-MgO buffered metal tape substrate with $\Delta\phi_{\text{MgO}} = 6.1^\circ$. (b) Out-of-plane XRD patterns of (i) BaFe₂As₂:Co epitaxial film grown on MgO single-crystal substrate (Film/sc-MgO), (ii) that on IBAD substrate with $\Delta\phi_{\text{MgO}} = 5.5^\circ$ (Film/IBAD) and (iii) bare IBAD substrate. Inset figure in (ii) shows an out-of-plane rocking curve of the 004 diffraction of a BaFe₂As₂:Co film on the IBAD substrate and the inset in (iii) illustrates the structure of IBAD substrates. (c) XRD pole-figure β scans of the BaFe₂As₂:Co 103 (top panel) and the MgO 022 diffractions (bottom panel) for Film/IBAD with $\Delta\phi_{\text{MgO}} = 5.5^\circ$. (d) The relationships between $\Delta\phi_{\text{BaFe}_2\text{As}_2:\text{Co}}$ of the 103 diffraction of the BaFe₂As₂:Co top and $\Delta\phi_{\text{MgO}}$ of the 022 diffraction of the MgO base-layer. The $\Delta\phi_{\text{BaFe}_2\text{As}_2:\text{Co}}$ of Film/sc-MgO with $\Delta\phi_{\text{MgO}} = 0.4^\circ$ is also shown by a triangle for comparison.

FIG. 2. (Color online) $\rho(T)$ of Film/IBAD (circles) and Film/sc-MgO (triangles). Inset figure shows the J - V characteristics at 2 K of Film/IBAD with (left) $\Delta\phi_{\text{MgO}} = 7.3^\circ$, (middle) 6.1° and (right) 5.5° .

FIG. 3. (Color online) (a) Magnetic field (H) dependences of J_c ($J_c(H//c)$) at 4 K (circles) and 12 K (triangles) of Film/IBAD with $\Delta\phi_{\text{MgO}} = 6.1^\circ$ (shown by red lines) and Film/sc-MgO (blue lines). (b) $J_c(H)$ measured in $H//ab$ and $H//c$ at temperatures of 4 K, 12 K, 16 K and 18 K indicated by red, orange, green and blue lines, respectively. Closed and open symbols correspond to $J_c(H//ab)$ and $J_c(H//c)$, respectively. Inset shows pinning force density (F_p) as a function of $\mu_0 H$ applied parallel to the c -axis at 4–18 K. The arrows in the inset show the $F_{p\text{max}}$ positions.

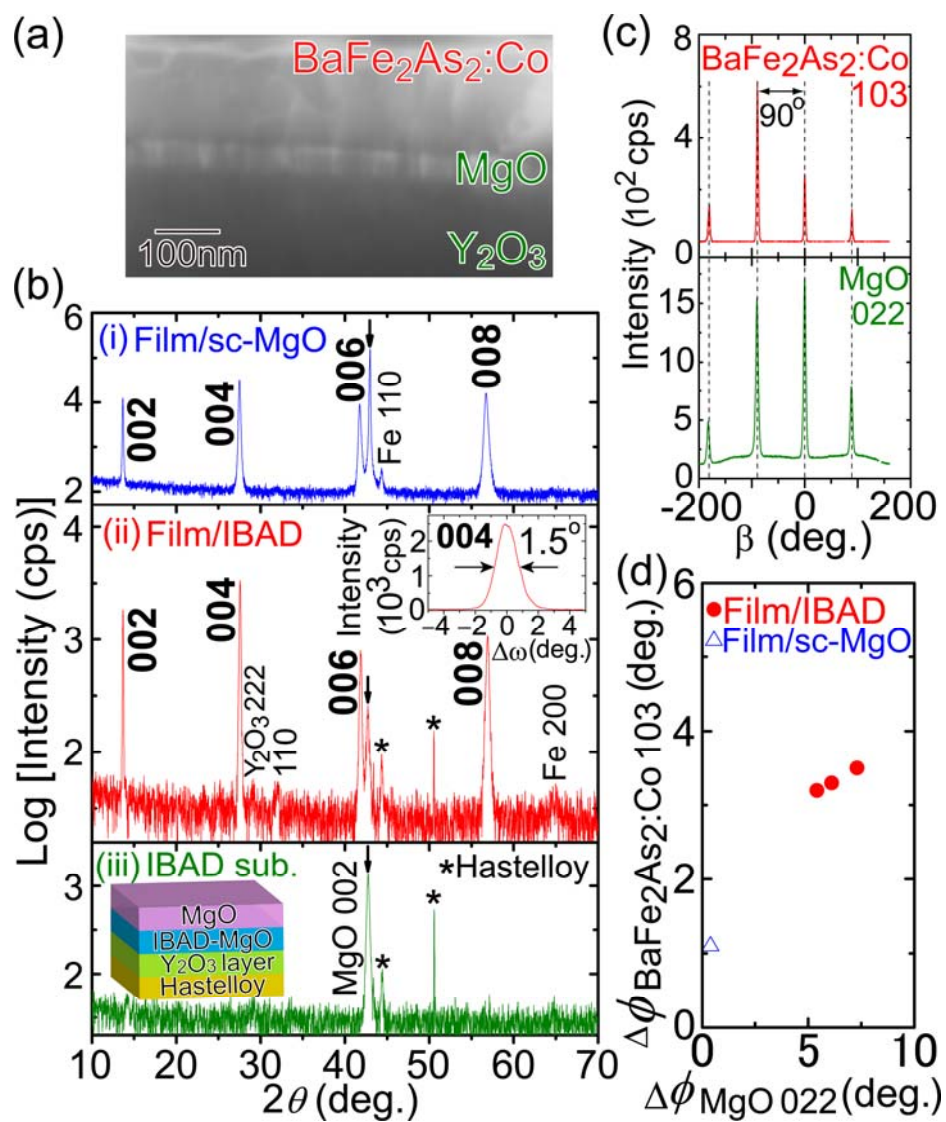


Figure 1

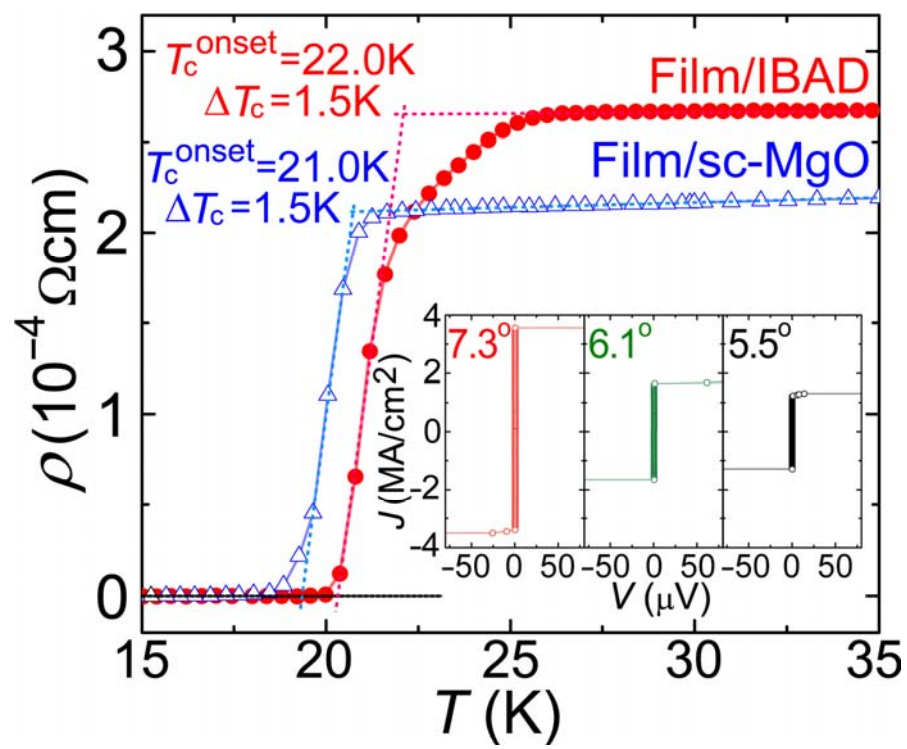


Figure 2

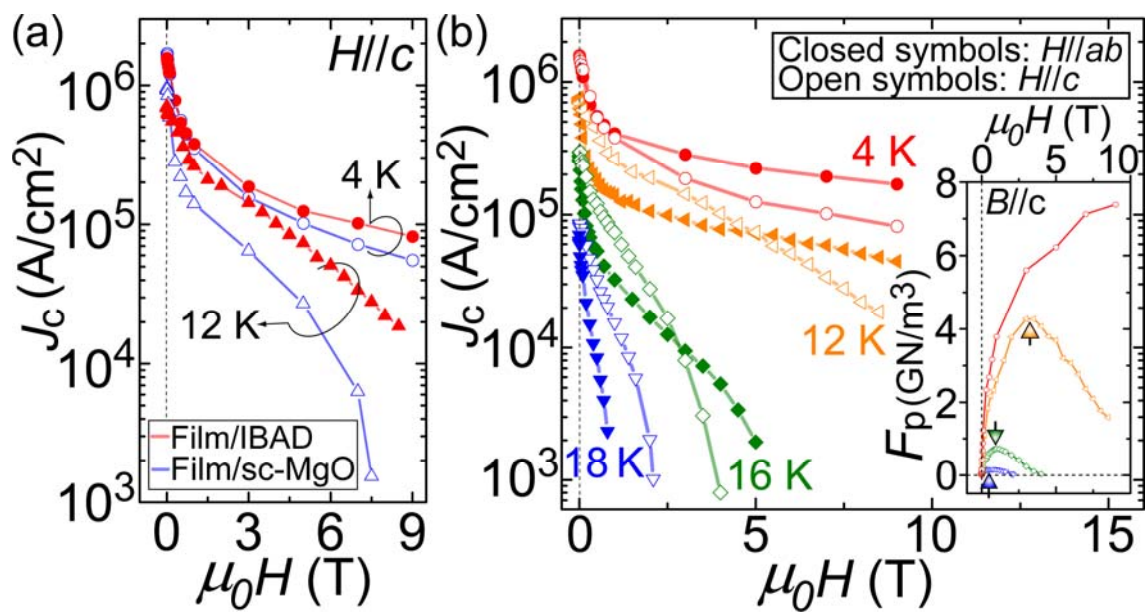


Figure 3